

Turbulent Convection and pulsational Stability of Variable Stars

I. Oscillations of Long-Period Variables

D. R. Xiong¹, L. Deng², & Q. L. Cheng¹

¹Purple Mountain Observatory, Academia Sinica, Nanjing 210008, P.R. China

²Beijing Astronomical Observatory, Academia Sinica, Beijing 100080, P.R. China

ABSTRACT

We have performed a linear pulsational stability survey of 6 series of long period variable models with $M = 1.0M_{\odot}$, $L = 3000 - 8000L_{\odot}$, and $(X, Z) = (0.700, 0.020), (0.735, 0.005)$. The dynamic and thermodynamic couplings between convection and oscillations are treated by using a statistical theory of nonlocal and time-dependent convection. The results show that the fundamental and all the low overtones are always pulsationally unstable for the low-temperature models when the coupling between convection and oscillations is ignored. When the coupling is considered, there is indeed a "Mira" pulsationally instability region outside of the Cepheid instability strip on the H-R diagram. The coolest models near the Hayashi track are pulsationally stable. Towards high temperature the fundamental mode first becomes unstable, and then the first overtone. Some one of the 2nd -4th overtone may become unstable for the hotter models. All the modes higher than 4th ($n > 4$) are pulsationally stable. The position and the width of such an instability region on the H-R diagram critically depends on the mass, luminosity and metal abundance of the star. The overall properties of the dependence are: 1) For the same mass and luminosity the instability region becomes slightly wider and moves to lower effective temperatures as the metal abundance increases; 2) For a given chemical abundance, the instability region becomes wider and moves to the lower effective temperature as their luminosity increases or their mass decreases

For the luminous red variables seated outside the instability strip the dynamic coupling between convection and oscillations balances or may even overtake the thermodynamic coupling. Turbulent viscosity can no longer be ignored for the pulsational instability of the low-temperature red variables. The effect of turbulent viscosity becomes more and more important for higher modes, and may finally become the main damping mechanism of the pulsation.

Subject headings: Convection - stars: Oscillations - stars: variables: long-period variables

1. Introduction

Observationally, there exists a group of low-temperature luminous pulsating red variables to the right of the Cepheid instability strip on the H-R diagram. They are the most heterogeneous red giants and super-giants belonging to both population I and II. On GCVS (General Catalogue of Variable Stars), these luminous red variables are categorized into 3 different types according to their variability: Miras (M), semi-regulars (SR) and slow irregular variables (L), among which, the first type (Miras) have been well studied. It is currently believed that the Miras are stars on the AGB stage of evolution. Detailed summaries of the observational properties and theoretical work on Miras have been given by Whitelock (1990) and Wood (1990a,b).

The nonlinear pulsation of Mira variables has been considered by Keeley (1970), Rose and Smith (1972), Wood (1974), Tuchman, Sack and Barkat (1978,1979), Hill and Willson (1979) Bowen (1988) and Perl and Tuchman (1990). The linear analysis is still useful for the stability survey. The linear pulsation of Mira variables were thoroughly studied by many authors (Kamijo 1962, Langer 1971, Fox and Wood 1982, Ostlie and Cox 1986, Balmforth Gough and Merryfield 1990, Cox and Ostlie 1991, Gong, Li and Huang 1995), among which Ostlie and Cox (1986) and Gong et al (1995) completely ignored the coupling between convection and oscillations. The coupling theory used by Kamijo, Langer, Fox and Wood, and Cox and Ostlie is over-simplified. Balmforth et al had used Gough's local time-dependent mixing length theory of convection in dealing with the coupling.

The red pulsating variables possess very extended convective envelopes. The convective energy transport in the H and He ionization regions well exceeds 99% of the total value. Convection overwhelms the κ -mechanism of radiation and becomes the principal excitation (damping) mechanism of pulsation. The local time-dependent theory of convection has been used to interpret the red edge of the Cepheid instability strip (Baker and Gough 1979, Xiong 1980). When the surface temperature decreases, the dynamical coupling (through turbulent pressure and turbulent viscosity) between convection and oscillations becomes more and more important (Xiong 1977, Gough 1977, Stellingwerf 1984). For red stars outside the Cepheid instability strip, the dynamical coupling between convection and oscillations becomes as powerful as the thermodynamic coupling. Precisely speaking, the local time-dependent theory of convection can no longer (at least in a self-consistent way) be used to treat the dynamical coupling. For this reason, we have developed a nonlocal time-dependent statistical theory of convection (Xiong 1989). In this paper we assumed that the convection is quasi-isotropic. Such an assumption excludes turbulent viscosity, which is anisotropic. We have developed a more precise version of the nonlocal time-dependent statistical theory of convection, in which the dynamic equations of the third order correlation functions are derived, and the anisotropy of turbulent convection is also considered (Xiong, Cheng & Deng 1997a). We have derived an equation of turbulent viscosity which is very similar to the Stokes equation of viscous fluid.

Comparing with previous works, the present version stands on a solid base of hydrodynamics

for describing the dynamic behavior of convective motion. Therefore, it would provide a better approach to both the dynamic and thermodynamic couplings between convection and oscillations. Using this new theory, in this paper we have performed a linear pulsational stability analysis for the luminous red stars outside the Cepheid instability strip. The working equations of linear non-adiabatic oscillations are given in Sect 2. Section 3 describes numerical results and theoretical arguments. A summary and concise conclusions of the present work are given at the end.

2. Working Equations

We have given a complete presentation of the nonlocal time-dependent theory of convection and all its mathematical formalism, i.e. the radiation-hydrodynamic equations of stellar oscillations (Xiong, Cheng & Deng 1997a). Among all the 14 equations, 3 deal with fluid motion (the conservation laws of mass, momentum and energy), 2 describe the radiation field (radiative transfer and energy conservation of the radiation field), and the other 9 equations are given for the second and the third correlation functions of turbulent velocity and temperature for turbulent convective motion. Within the frame work of the Eddington approximation, the departure from radiative equilibrium has been accurately taken into account. The gas and radiation are treated separately, and they become coupled through the absorption and emission processes of matter. In the mean time, careful consideration has been given to the anisotropy of turbulence and the inertia of turbulent convection. The turbulent viscosity, which is nearly identical in form to the Stokes formula for viscous fluid, is included automatically in the dynamic equation of the second-order correlation of turbulent velocity. When we adopt a simplified gradient-type diffusion approximation for the third-order correlations, this reduces the number of radiation-hydrodynamic equations down to 11. We have computed the linear non-adiabatic radial oscillations of p-modes for a solar model using these simplified radiation-hydrodynamic equations. The results show that the effects of departure from radiative equilibrium are negligible only except for very high order p-mode ($n \geq 25$) (Cheng & Xiong 1997). In this work, we will ignore the departure from radiative equilibrium. In the context of the present study this is safe, because the giants and super-giants almost always pulsate at low-order modes. Assuming that the gas and the radiation field are always in equilibrium, we can treat them together. In this way, the number of equations is reduced down to 10 and the pulsational equations are greatly simplified. Under such circumstances, the linear non-adiabatic equations can be written as

$$\frac{dy_3}{d \ln r} + 3y_3 + \delta y_1 - \alpha y_2 = 0, \quad (1)$$

$$\begin{aligned} & \frac{d}{d \ln r} \left[(P + \delta \rho x^2) y_1 + \rho x^2 (2y_5 - \alpha y_2) \right] \\ & + \frac{1}{r^3} \frac{d}{d \ln r} \left\{ \left[\frac{GM_r \rho r \alpha V \tau_c}{4} + \frac{4}{3} \frac{i \omega \tau_c^*}{1 + i \omega \tau_c^*} \left(\rho r^3 x^2 + \frac{GM_r \rho r \alpha V \tau_c}{4} \right) \right] (\delta y_1 - \alpha y_2 + 3y_3) \right\} \end{aligned}$$

$$\begin{aligned}
& + \frac{4GM_r \rho r \alpha V \tau_c^*}{3(1+i\omega\tau_c^*)} \left[y_9 - \left(2 + \frac{r^3 \omega^2}{GM_r} + \frac{3}{8} i\omega\tau_c \right) y_3 \right] \Big\} \\
& - \left\{ \frac{3}{4r^3} \frac{d}{d \ln r} (GM_r \rho r \alpha V \tau_c) + 4 \frac{GM_r \rho}{r} + \rho r^2 \omega^2 \right\} y_3 = 0,
\end{aligned} \tag{2}$$

$$\frac{dy_2}{d \ln r} - \frac{d \ln T}{d \ln r} [\chi_P y_1 + (\chi_T - 4) y_2 - 4y_3 + y_4] = 0, \tag{3}$$

$$\begin{aligned}
& \frac{d}{d \ln r} \left\{ 3y_6 + \frac{L_c}{L} [(\delta + C_{p,P}) y_1 + (1 - \alpha + C_{p,T}) y_2 + 2y_3 + y_9] + \frac{L_r}{L} y_4 \right\} \\
& + i\omega \frac{4\pi r^3 \rho C_p T}{L} \left[3 \frac{x^2}{C_p T} y_5 - \left(\nabla_{\text{ad}} + \frac{\delta x^2}{C_p T} \right) y_1 + \left(1 + \frac{\alpha x^2}{C_p T} \right) y_2 \right] = 0,
\end{aligned} \tag{4}$$

$$\frac{\sqrt{3}\pi c_2 r^3 P x^3}{GM_r L} \frac{dy_5}{d \ln r} - \frac{L_1}{L} \{(1 + \delta) y_1 - \alpha y_2 + 6y_3 + 3y_5 - y_6\} = 0, \tag{5}$$

$$\begin{aligned}
& \frac{\sqrt{3}\pi c_2 r^3 \rho C_p^2 P x Z}{GM_r} \frac{dy_7}{d \ln r} - L_3 \{[1 + 2(\delta + C_{p,P})] y_1 + 2(C_{p,T} - \alpha) y_2 \\
& + 6y_3 + y_5 + y_7 - y_8\} = 0,
\end{aligned} \tag{6}$$

$$\begin{aligned}
& \frac{\sqrt{3}\pi c_2 r^3 \rho C_p P x V}{GM_r} \frac{dy_9}{d \ln r} - L_5 \{[1 + \delta + C_{p,P}] y_1 + (C_{p,T} - \alpha) y_2 \\
& + 6y_3 + y_5 + y_9 - y_{10}\} = 0,
\end{aligned} \tag{7}$$

$$\begin{aligned}
& \frac{1}{L} \frac{d(L_1 y_6)}{d \ln r} + \frac{4\pi GM_r \rho r}{3L} \left\{ \left[\left(\delta - 1 - \frac{\delta}{2} i\omega\tau_c \right) \frac{1.56\rho x^3}{c_1 P} - \alpha V \left(\alpha_p + \frac{\delta}{4} i\omega\tau_c \right) \right] y_1 \right. \\
& + \alpha \left[\left(\frac{1}{2} i\omega\tau_c - 1 \right) \frac{1.56\rho x^3}{c_1 P} + V \left(\frac{1}{4} i\omega\tau_c - \alpha_T \right) \right] y_2 \\
& + \left[\alpha V \left(2 + \frac{r^3 \omega^2}{GM_r} - \frac{3}{4} i\omega\tau_c \right) - 2 \frac{1.56\rho x^3}{c_1 P} \right] y_3 \\
& \left. 3 \left(1 + \frac{1}{2} i\omega\tau_c \right) \frac{1.56\rho x^3}{c_1 P} y_5 - \alpha V y_9 \right\} = 0,
\end{aligned} \tag{8}$$

$$\begin{aligned}
& \frac{1}{4\pi r^2 \rho^2 C_p^2} \frac{d(L_3 y_8)}{d \ln r} + 2V \left\{ \frac{dy_2}{d \ln r} - \nabla_{\text{ad}} \frac{dy_1}{d \ln r} + \left(\frac{d \ln T}{d \ln r} - \nabla_{\text{ad}} \frac{d \ln P}{d \ln r} \right) y_9 \right\} \\
& - 2 \left[\frac{\delta + C_{p,P}}{4\pi r^2 \rho^2 C_p^2} \frac{dL_3}{d \ln r} + V \nabla_{\text{ad}} \nabla_{\text{ad},P} + \frac{GM_r \rho Z}{c_1 r \rho} (x + x_c + \nabla_{\text{ad}} \alpha_T \sqrt{3} \eta_e i \omega \tau_c x) \right] y_1 \\
& + 2 \left[\frac{\alpha - C_{p,T}}{4\pi r^2 \rho^2 C_p^2} \frac{dL_3}{d \ln r} + i \omega \tau_c \sqrt{3} \eta_e \frac{GM_r \rho x Z}{c_1 r P} \right] y_2 \\
& + 4 \left[\left(\frac{d \ln T}{d \ln r} - \nabla_{\text{ad}} \frac{d \ln P}{d \ln r} \right) V - \frac{GM_r \rho}{c_1 r P} (x + x_c) Z \right] y_3 \\
& + \frac{GM_r \rho Z}{c_1 r \rho} \left\{ 2x y_5 + \left[2(x + x_c) + i \omega \tau_c \sqrt{3} \eta_e x \right] y_7 \right\} = 0, \tag{9}
\end{aligned}$$

$$\begin{aligned}
& \frac{1}{4\pi r^2 \rho C_p} \frac{d(L_5 y_{10})}{d \ln r} + x^2 \left(\frac{dy_2}{d \ln r} - \nabla_{\text{ad}} \frac{dy_1}{d \ln r} \right) + i \omega \tau_c \frac{\sqrt{3} \eta_e GM_r \rho x V}{c_1 r P} \frac{dy_3}{d \ln r} \\
& - \left[\frac{\delta + C_{p,P}}{4\pi r^2 \rho C_p} \frac{dL_5}{d \ln r} + x^2 \nabla_{\text{ad}} \nabla_{\text{ad},P} + \frac{GM_r \rho V}{c_1 r P} (2.56x + x_c + i \omega \tau_c \sqrt{3} \eta_e \nabla_{\text{ad}} \alpha_T x) \right] y_1 \\
& + \left[\frac{\alpha - C_{p,T}}{4\pi r^2 \rho C_p} \frac{dL_5}{d \ln r} + i \omega \tau_c \sqrt{3} \eta_e (1 - \alpha + C_{p,T}) \frac{GM_r \rho x V}{c_1 r P} \right] y_2 \\
& + \left\{ \frac{GM_r \alpha Z}{r} \left(2 + \frac{r^3 \omega^2}{GM_r} \right) + \frac{GM_r \rho V}{c_1 r P} [i \omega \tau_c \sqrt{3} \eta_e x - 2(2.56x + x_c)] \right. \\
& \left. + 2x^2 \left(\frac{d \ln T}{d \ln r} - \nabla_{\text{ad}} \frac{d \ln \rho}{d \ln r} \right) \right\} y_3 + \left[2x^2 \left(\frac{d \ln T}{d \ln r} - \nabla_{\text{ad}} \frac{d \ln P}{d \ln r} \right) + 2.56 \frac{GM_r \rho x V}{c_1 r P} \right] y_5 \\
& - \frac{GM_r}{c_1 r P} \alpha Z y_7 + \frac{GM_r \rho V}{c_1 r P} (2.56x + x_c + i \omega \tau_c \sqrt{3} \eta_e x) y_9 = 0, \tag{10}
\end{aligned}$$

where

$$\begin{aligned}
y_1 &= \frac{\delta P}{P}, & y_2 &= \frac{\delta T}{T}, & y_3 &= \frac{\delta r}{r}, & y_4 &= \frac{\delta L_r}{L_r}, & y_5 &= \frac{\delta x}{x}, \\
y_6 &= \frac{\delta L_1}{L_1}, & y_7 &= \frac{\delta Z}{Z}, & y_8 &= \frac{\delta L_3}{L_3}, & y_9 &= \frac{\delta V}{V}, & y_{10} &= \frac{\delta L_5}{L_5}
\end{aligned} \tag{11}$$

are the relative complex amplitudes of pulsation. x , Z and V are the auto- and cross-correlation functions of turbulent velocity and temperature fluctuation respectively,

$$x^2 = \sum_{i=1}^3 \overline{w_i' w_i'} / 3, \quad Z = \overline{T'^2} / \bar{T}^2, \quad V = \overline{w_r' T'} / T, \tag{12}$$

and $\tau_c^* = \frac{3}{16}\tau_c$. τ_c is the inertial time scale for turbulent convection, which is

$$\tau_c = \frac{c_1 Pr^2}{\sqrt{3}\eta_e GM_r \rho x},$$

while L_1 , L_3 and L_5 are the convective variables relevant to the third correlations. c_1 and c_2 are respectively the two convective parameters relevant to the dissipation and diffusion of turbulence. In our statistical theory of turbulent convection (Xiong 1980,1989), $l_e = c_1 Hp$ (Hp is the local pressure scale height) is the average size of energy-containing eddies. $\epsilon = 2\eta_e x^3/l_e$ (η_e is the Heisenberg eddy-coupling constant) is the turbulent dissipation (Hinze 1975). $l = c_2 Hp$ is the turbulent diffusion length scale. The e-folding length of convective overshooting is about $1.4\sqrt{c_1 c_2} H_P$ (Xiong 1985). α and δ are the coefficients of expansion and compression for the gas. Variables with a subscript "P" (or "T") denote the logarithm partial derivative with respect to "P" (or "T"), such as:

$$\chi_T = \left(\frac{\partial \ln \chi}{\partial \ln T} \right)_P.$$

More detailed definitions concerning the above expressions have been given in our previous work (Cheng & Xiong 1997). One thing that should be made clear is that the gas and radiation are treated as a whole ($P = P_g + P_r$) in the present work, differing from our previous manner. Therefore, the contribution by radiation to all the material properties and to all the thermodynamic quantities, such as δ , α , C_p and ∇_{ad} , has been included.

The boundary conditions at the bottom layer are:

$$y_3 = 0, \tag{13}$$

$$y_2 = \nabla_{\text{ad}} y_1, \tag{14}$$

$$y_6 = \sqrt{\frac{12\sqrt{3}\eta_e}{1 + 2\sqrt{3}\eta_e}} (2 + i\omega\tau_c) y_5, \tag{15}$$

$$y_8 = \sqrt{\frac{12\sqrt{3}\eta_e}{1 + 2\sqrt{3}\eta_e}} \left(\frac{2}{\sqrt{3}\eta_e} + i\omega\tau_c \right) y_7, \tag{16}$$

$$y_{10} = \sqrt{\frac{12\sqrt{3}\eta_e}{1 + 2\sqrt{3}\eta_e}} \left(2 + \frac{1}{\sqrt{3}\eta_e} + i\omega\tau_c \right) y_9, \tag{17}$$

and the boundary conditions at the surface are,

$$y_3 = 1, \tag{18}$$

$$y_1 + \left(4 + \frac{r^3 \omega^2}{GM_r}\right) y_3 = 0, \tag{19}$$

$$4y_2 + 2y_3 - y_4 = 0, \tag{20}$$

$$y_6 = \sqrt{\frac{12\sqrt{3}\eta_e}{1 + 2\sqrt{3}\eta_e}} (2 + i\omega\tau_c) y_5, \tag{21}$$

$$y_8 = \sqrt{\frac{12\sqrt{3}\eta_e}{1 + 2\sqrt{3}\eta_e} \left(\frac{2}{\sqrt{3}\eta_e} + i\omega\tau_c\right)} y_7, \tag{22}$$

$$y_{10} = \sqrt{\frac{12\sqrt{3}\eta_e}{1 + 2\sqrt{3}\eta_e} \left(2 + \frac{1}{\sqrt{3}\eta_e} + i\omega\tau_c\right)} y_9, \tag{23}$$

As we have done in the previous paper (Cheng & Xiong 1997), the lower boundary is set in the convective overshooting zone, and the upper one is taken to be optically thin enough in the stellar atmosphere. Explicitly, we have adopted an optical depth of $\tau = 0.01$ for the upper boundary in the present work.

The convective boundary conditions Eqs. (15)–(17) and (21)–(23) are given by the asymptotic analysis of the convective quantities within the overshooting zone. For their details we refer to our another work by Xiong et al (1997b), where the spatial oscillations of convective variables are amply discussed.

3. The Numerical Results

We have calculated the linear non-adiabatic pulsation for 6 series of models of luminous red stars. Their masses, luminosities, chemical compositions and of pulsational instability region are listed in Table 1. The convective parameters are $c_1 = c_2 = 0.75$, this leads about the same energy transport efficiency as the original Vitense theory (Vitense 1958) when the mixing-length is taken to be one and half of the local pressure scale height, i.e. $l = 1.5H_P$, and the e-folding length of convective overshooting is about $1.4\sqrt{c_1 c_2} H_P \approx 1.05H_P$. The reddest model in the series is very close to the corresponding Hayashi track, while for the hottest model the convective flux is much smaller than the radiation flux in the second ionization region of helium. For these hotter stars,

the κ -mechanism functioning in the second ionization region of helium has already operated, and it has become the main excitation mechanism. Therefore, our models actually cover all the possible temperatures of the luminous red stars outside the Cepheid instability strip, for the present setting of mass, luminosity and chemical composition.

In the present work we use a simplified MHD equation of state (Hummer and Mihalas 1988, Mihalas et al. 1988, Dappen et al. 1988). The neutral helium has been considered as a hydrogen-like atom for convenience of calculation of its energy levels. A significant departure only appears in the ground and the lower excited states. An analytic approach to the OPAL tabular opacities (Rogers and Iglesias 1992) and the low-temperature tabular opacities (Alexander 1975) is used for the calculation of opacity.

3.1. "Mira" Instability Strip

Table 2 gives the linear amplitude growth rates of the model series 2 of luminous red stars, $\eta = -2\pi\omega_i/\omega_r$, where $\omega = \omega_r + i\omega_i$ is the complex angular frequency of linear non-adiabatic oscillations. The first column is the serial number of the model, the second is the effective temperature T_e , the 3rd-7th columns are the amplitude growth rates for the fundamental through 4th overtones (taking into account the coupling between convection and oscillations). We have actually calculated the first 12 modes ($n = 0 - 11$) for non-adiabatic oscillations. However, all the modes with $n > 4$ are pulsationally stable for luminous red stars. For the sake of clarity, we give in Table 2 only the first five modes. Aimed at examining the effect of convection on the pulsational instability for red stars, we have also computed the non-adiabatic pulsation ignoring the coupling between convection and oscillations (however, convection has been included in the static models). If convection does not vary during the oscillation of a star, the convective variables $y_5 = y_6 = y_7 = y_8 = y_9 = y_{10} = 0$, Eqs. (5)–(10) and the convective boundary conditions Eqs. (15)–(17) and (21)–(23) can be omitted. Omitting the terms related to convection, Eqs. (2) and (10) are reduced to

$$\frac{d}{d \ln r} (P y_1) - \left(4 \frac{GM_r \rho}{r} + \rho r^2 \omega^2 \right) y_3 = 0, \quad (24)$$

$$\frac{d}{d \ln r} \left(\frac{L_r}{L} y_4 \right) - i\omega \frac{4\pi r^3 \rho C_p T}{L} (\nabla_{\text{ad}} y_1 - y_2) = 0. \quad (25)$$

The number of pulsational equations reduces down to 4. That is the decoupling between convection and oscillations. Eqs. (1), (3) (24), (25) and the boundary conditions Eqs. (13), (14), and (18)–(20) were used to calculate the non-adiabatic pulsation of stars ignoring the coupling between convection and oscillations. The corresponding growth rates of the first five modes

($n = 0 - 4$) are given as the 8–12th columns in Table 2. Depicted in Fig. 1 are the variations of the amplitude growth rates of the fundamental mode and the first overtone against the stellar effective temperatures for the 6 model series.

It is clear from Table 2 and Fig. 1 that, when excluding the coupling between convection and oscillations, the fundamental mode, the first overtone and most of the low order overtone are pulsationally unstable for all the models of luminous red stars. But this is not true. Obviously, this is due to the ignorance of the coupling between convection and oscillations. More generally speaking, no good interpretation can be made for the red edge of the Cepheid instability strip if one does not take such coupling into consideration (Iben 1966, Xiong 1980).

When the coupling between convection and oscillations is considered, most of the low order modes and all the higher order modes ($n > 4$) become pulsationally stable. However, there does exist a pulsationally unstable region for the luminous red stars outside the Cepheid instability strip. The coolest models near the Hayashi track are pulsationally stable. Towards high temperature the fundamental mode first becomes unstable, and then the first overtone. Some one of 2nd -4th overtones may become unstable for the hotter models. All the modes higher than the 4th ($n > 4$) are pulsationally stable. For simplicity, and to make it distinct with the other pulsationally unstable region, we will call it "Mira instability strip" for the moment, though such a name may not be very appropriate. This instability strip includes not only the regulars Miras, but also the semi-regular and irregular variables.

Our calculations show that the pulsational instability of a luminous red star depends critically on stellar metal abundance, luminosity and mass. The overall properties are:

1. For the same mass and luminosity, the instability strip becomes slightly wider and its location moves to lower effective temperature in the H-R diagram as the metal abundance increases.
2. For the same abundance, the instability strip becomes slightly wider and its location moves to lower effective temperature in the H-R diagram as the the luminosity increases or the mass decreases.

The above characteristics of luminous red variables are closely connected with the structure of the convective zones of these stars. Convection is the dominant factor that controls the pulsational instability for red stars. H_2O and TiO contribute most of the absorption in the low temperature region, therefore the low temperature opacity strongly depends on the metal abundance. Moreover, the structure of the stellar convective zone is determined by the nature of the outermost super-adiabatic layer, hence the extension of the convective zone depends critically on the metal abundance. That explains why the Mira instability strip and the Hayashi track move to lower temperature as metal abundance increases. In the mean time, the structure of the convective zone depends also on the mass and luminosity. The above reasons make it easy to understand the properties of the Mira instability strip.

3.2. Excitation and Damping of Oscillations

For the luminous red stars outside the instability strip, the convective energy transport exceeds 99% of the total quantity in the ionization regions of hydrogen and helium. Fig. 2 and Fig. 3 give the integrated work W_P versus depth for the luminous stars pulsating at the fundamental mode. In Fig. 2, convection has been included for the static model, while the coupling between convection and oscillations is ignored in calculations of non-adiabatic oscillations. The only excitation and damping mechanism results from radiation. It can be found from Fig. 2 that for the two cooler models the excitation comes mainly from the the outermost gradient region of radiation flux, where χ_T approaches its maximum. This excitation mechanism functioning in the gradient region of radiation flux will be detailed in our second paper (Xiong, Cheng & Deng 1997b). The radiative excitation arising in the second ionization region of helium becomes negligible, because the radiative flux is far smaller than the convective flux here. The radiative excitation occurring in the second ionization region of helium becomes unneegligible for the hotter model. For a clearer display, the variation of χ_T and $\log(L_r/L)$ in the stellar interior are given in Fig. 2 as well. Due to the convective energy transport, the radiative damping in the deep interior of a star is greatly weakened. Hence, the star is always pulsationally unstable when the coupling between convection and oscillations is ignired.

Fig. 3 plots the quantities for the same luminous red star model, but with the coupling between convection and oscillations being considered. W_P , W_{Pt} and W_{vis} represent respectively the contributions of the gas (and radiation) pressure, turbulent pressure, and turbulent viscosity. Their exact definitions are referred to our previous work (Cheng & Xiong 1997). $W_{all} = W_p + W_{Pt} + W_{vis}$ is the total integrated work, the value of which at the surface of a star should be the amplitude growth rate $\eta = -2\pi\omega_i/\omega_r$ given by the non-adiabatic pulsation calculation. Our results show that they are very closely matched indeed.

By comparing Figs. 2 and 3, one can see that their characteristics are totally different. It can be found from Fig. 3 that with consideration of the coupling between convection and oscillations the excitation (and damping) region of pulsation, where W_{all} changes obviously, extends deeper into stellar interior in comparition with Fig. 2. This is surely a result of the coupling between convection and oscillations.

Convection leads to energy and momentum exchange inside a star, and hence affects the pulsational instability for variable stars. We call the effects of convective energy transport on variable stars as thermodynamic coupling, while the effect of momentum exchange on variable stars as dynamic coupling.

The gas (and radiation) pressure term W_P in the total integrated work contains the effect of energy transport not only by radiation, but also by convection (i.e. the contribution by thermodynamic coupling between convection and oscillations). It is hard to unambiguously separate the effects of convective energy transport from radiative transport, because the two factors are closely coupled in the process of stellar oscillations. Following the conservation law

of energy (momentum), any change in convective flux (turbulent pressure) must lead to the corresponding change in the radiation flux (gas pressure) in order to balance the previous factor, and visa versa. By the same reason, it is not so easy to separate unambiguously the contribution of gas (and radiation) pressure W_P from that of the turbulent pressure W_{Pt} .

The combination of W_{Pt} and W_{vis} is the dynamic coupling between convection and oscillations. The effect of turbulent viscosity is to convert the kinetic energy of ordered pulsation into random turbulent kinetic energy, and this process happens in the low wave number region of turbulent energy spectra . Through the nonlinear effects of fluid dynamics, the energy gained in the pulsational motion is cascaded into higher and higher wave number regions, and is eventually converted into thermal energy at the smallest turbulent eddies. Therefore the turbulent viscosity always works as a damping factor to pulsation, i.e. W_{vis} is always negative. Although W_{vis} is far less than W_P and W_{Pt} in absolute values for the fundamental mode of luminous red stars, we cannot ignore its effect on the stability of pulsation. The contribution of turbulent viscosity increases very quickly towards higher modes for luminous red variables because viscous dissipation is proportional to the square of velocity gradient which grows as the oscillation mode increases. The turbulent viscosity becomes the main damping mechanism of the high overtones. This is the reason why the luminous red stars become pulsationally stable at high modes. Fig. 4 demonstrates the integrated work diagram for the first, 3rd and 5th modes of a $T_e = 2550K$ model. Fig. 3a and Fig. 4 clearly show the quick increase of W_{vis} towards higher modes.

The coupling between convection and oscillations depends critically on the ratio of the time-scale of convective motion τ_c to that of pulsation $\tau_p = 2\pi/\omega_r$, i.e. $\omega_r\tau_c$. When τ_c is much smaller than τ_p , i.e. $\omega_r\tau_c \ll 1$, the convection is in nearly quasi-steady variation. When $\omega_r\tau_c$ increases, convection lags behind the pulsational variation. The result is that not only its variation amplitude decreases, but also a phase lag exists. The interaction between convection and oscillations depends on both the amplitude of the convective variations and the phase of such variations. As we will show later on (Xiong, Cheng & Deng 1997b), the τ_c distribution in the interior of luminous red giants is very different from that of the RR Lyrae and the horizontal branch red stars. This difference results from the difference of their mass- luminosity ratios between them. The long-period variables have very low mass-luminosity ratio. Therefore, their internal structure has very high central concentration. This may explain the difference in pulsational characteristics of these two kinds of stars. In Figs. 3 and 4 we have also given the curves for $\omega_r\tau_c$ versus depth ($\log T$). This shows that, for such luminous red stars, $\omega_r\tau_c \leq 1$ holds for most of the interior of envelope model except the extremely outermost layer.

4. Conclusions and Discussion

By using a nonlocal and time-dependent theory of convection, we have very carefully treated the coupling between convection and oscillations. The linear stability analysis for luminous red stars gives us the following results:

1. The coupling between convection and oscillations is the dominant factor for the pulsational instability. When this coupling is not considered, all the low-temperature red stars are pulsationally unstable, while when it is taken into account, a Mira instability strip will show up outside the Cepheid instability strip;
2. Except for some slightly hotter models which may have pulsationally unstable second to fourth overtone modes, luminous red variable stars pulsate in the fundamental mode or the first overtone. All the modes higher than 4 are pulsationally stable;
3. For the low-temperature red stars, the dynamic coupling between convection and oscillations is in the same order of magnitude as the thermodynamic coupling, and may even overtake the later;
4. The effect of turbulent viscosity grows very quickly towards high overtones for the luminous red stars. For high overtones, it becomes the main damping mechanism.

The troublesome spatial oscillations of the thermodynamic quantities are triggered when the local time-dependent convection theory is used in calculating the stellar oscillations. (Keeley 1977, Baker & Gough 1979, Gonczi & Osaki 1980). In the present calculations of the nonlocal convection time-dependent theory the spatial oscillations still exist but are effectively controlled. For the model of luminous red variable stars, the spatial oscillations happen at the extreme outer layer of the atmosphere, where $\omega\tau_c \gg 1$. In the stellar interiors, where $\omega\tau_c < 1$, the troublesome spatial oscillations do not appear. It is difficult to trace the spatial oscillations in Figs. 3 and 4, since the convective energy transport is far less than the radiative energy transport, and the turbulent pressure is far less than the gas pressure in the atmosphere of a luminous red giant. It seems true that the spatial oscillations do not affect the pulsation instability of luminous red stars to a considerable level.

As for the long disputed pulsational mode for O Ceti, some authors think that O Ceti is pulsating in the first overtone (Kamijo 1962, Keeley 1970, Wood 1974 & 1981, Tuchman, Sack & Barkat 1978, Tuchman 1991), while some others believe that it oscillates in the fundamental mode (Hill & Willson 1979, Willson 1982, Bowen 1988). The theoretical pulsation period P and pulsation constant Q for a luminous red star model, with $L = 5000L_\odot$, $X = 0.700$, $Z = 0.020$, are given in Table 3. Fig. 5 gives the P and Q of the fundamental and first modes versus the effective temperature for 6 model series. Our theoretical value of the pulsation constant Q is very close to that of Ostlie & Cox (1986), but our Q_1 for the first overtone is systematically smaller than that of Wood (1982) especially at the long period end. Following our numerical results, there is no model having its first overtone Q_1 that exceeds 0.045 days. Normally, $Q_1 \leq 0.041$. Assuming for O Ceti, $M \approx M_\odot$, $T_e = 2900K$ (Wood 1990a,b) and that it pulsates at the first overtone, then we have $L \approx 12500L_\odot$ or $M_{bol} \approx -5.5$. This would make it 0.7^m more luminous than the value of $M_{bol} = -4.8$ given by the P-L relation for Miras in the Large Magellanic Cloud (Glass et al 1987, Hughes & Wood 1990). This is unlikely to be real. Wood (1996b) proposed another picture for O

Ceti. If Mira's P-L relation depends on the metal abundance, then the discrepancy between the observed and the theoretical Q values could be removed. Our results of linear pulsational stability survey support Wood's guess. The instability strip moves indeed towards the low temperature as the metal abundance increases, as shown by Table 1 and Fig. 1. Our calculations show that if the metal abundance for LMC Miras are only one-half of that of O Ceti the red edge of the Mira instability strip in the Galaxy will be lowered by about $350K$ compared with the LMC's. Therefore the magnitude of O Ceti derived from the LMC P-L relation will be 0.6^m more luminous than it actually is. Let us suppose that the effective temperature of O Ceti is $T_e = 2900K$ and $M_{bol} = -4.2$, then the pulsation period of the fundamental mode given by the non-adiabatic calculation will be 330 days. Following our linear stability analysis, it appears more likely for O Ceti to pulsate in the fundamental mode than in the first overtone.

This work is supported in part by the contract number 19573018 of National Natural Science Foundation of China (NSFC).

REFERENCES

- Alexander, D.R., 1975, ApJS, 29, 363
- Baker, N. and Gough, D.O., 1979, ApJ, 234, 232
- Balmforth, N.J., Gough, D.O. and Merryfield, W.J., 1990. in *From Miras to Planetary Nebulae*, eds. Mennesier, M.O. and Omont, A. (Editions Frontieres), p. 85
- Bowen, G.H., 1988, ApJ, 329, 299
- Cheng, Q.L. and Xiong, D.R., 1997, A&A, 319, 981
- Cox A.N. and Ostlie, D.A., 1991, Astrophys. Spac. Sci, 210, 311
- Dappen, W., Mihalas, D., Hummer, D.G., and Mihalas, b.W., 1988, ApJ, 332, 261
- Fox, M.W., and Wood, P.R., 1982, ApJ, 259, 198
- Glass, I.S., Catchpole, R.M., Feast, M.W., Whitelock, P.A. and Reid, I.N., 1987, in *In the Late Stages of Stellar Evolution*, eds. Kwok, S. and Pottasch, S. R., (Reidel), p. 51
- Gonczi, G., and Osaki, Y., 1980, A&A, 84, 196
- Gong, Z.G., Li, Y. and Huang, R.Q., 1995, Acta Astrophys. Sinica, 15, 56
- Gough, D.O., 1977, ApJ, 214, 196
- Hill, S.J. and Willson, L.A., 1979, ApJ, 229, 1029
- Hinze, J.O., 1975 Turbulence, second edition (McGran-Hill Book Company, New York)
- Hughes, S.M.G., and Wood, P.R., 1990, AJ, 99, 784
- Hummer, D.G. and Mihalas, D., 1988, ApJ, 331, 794

- Iben, I.Jr., 1996, ApJ, 166, 131
- Kamijo, F., 1962, PASJ, 14, 271
- Keeley, D.A., 1970, ApJ, 161, 657
- Keeley, D.A., 1977, ApJ, 221, 926
- Langer, G.E., 1971, MNRAS, 155, 199
- Mihalas, D., Dappen, W. and Hummer, D.G., 1988, ApJ, 331, 815
- Ostlie, D.A. and Cox, A.N., 1986, ApJ, 311, 864
- Perl, M. and Tuchman, Y., 1990, ApJ, 360, 554
- Rogers, F. and Iglesias, C.A., 1992, ApJS, 79, 507
- Rose, M. and Smith, R. L., 1972, ApJ, 159, 903
- Stellingwerf, R.F., 1984, ApJ, 277, 322
- Tuchman, Y. Sack, N. and Barkat, Z., 1978, ApJ, 219, 183
- Tuchman, Y. Sack, N. and Barkat, Z., 1979, ApJ, 234, 217
- Tuchman, Y., 1991, ApJ, 383, 778
- Vitense, E., 1958, Z. Astrophys., 46, 108
- Whitlock, P.A., 1990, A.S.P. Conf. Ser. Vol. 11, eds Cacciari, C., and Clementini, G., (San Francisco, CA), p. 365 (Boulder:Joint Institute for Laboratory Astrophysics), p. 284
- Willson, L.A., 1982, in *Pulsations in Classical and Cataclysmic Variables*, eds. Cox, J.P. and Hansen, C.J.
- Wood, P.R., 1974, ApJ, 190, 609
- Wood, P.R., 1981, in *Physical Processes in Red Giants*, eds. Iben, I.Jr., and Renzini, A. (Dordrecht:Reidel), p. 205
- Wood, P.R., 1990a, in *From Miras to Planetary Nubulae* ed. Mennesier, M.O. and Omont, A. (Editions Frontieres), p. 67
- Wood, P.R., 1990b, in *A.S.P. Conf. Ser. Vol 11*, eds. Cacciari, C. and Clementini, G. (San Francisco, CA), p355
- Xiong, D.R., 1977, Act Astron. Sinica, 18, 86 (=Chinese Astron., 2, 118)
- Xiong, D.R., 1980, Scientia Sinica, 23, 1139
- Xiong, D.R., 1985, A&A, 150, 133
- Xiong, D.R., 1989, A&A, 209, 126
- Xiong, D.R., Cheng, Q.L. and Deng, L., 1997a, ApJS, 108, 529
- Xiong, D.R., Cheng, Q.L. and Deng, L., 1997b, submitted to ApJ

Figure Captions

Fig. 1.— The amplitude growth rate of pulsation for the fundamental mode and the first overtone varies with the effective temperature, *with conv.* and *without conv.* denote the cases when the coupling between convection and oscillations are included and not included respectively.

Fig. 2.— The variations of the integrated work W_p (solid line), Γ_2 (dotted), χ_T (dashed), and $\log(L_r/L)$ with respect to depth ($\log T$) for three models of model series 2 ($M = 5000M_\odot$, $L = 5000L_\odot$, $X = 0.700$, $Z = 0.020$). The coupling between convection and oscillations is ignored in the pulsation calculation, while convection is included for the corresponding static models. The three horizontal lines are the locations of the ionization regions of H and He.

Fig. 3.— The integrated work vs. depth ($\log T$) for the same models as in Fig. 2, however the coupling between convection and oscillations is included. W_P , W_{Pt} and W_{vis} are respectively the components by gas (and radiation) pressure, turbulent pressure and turbulent viscosity. The variations of $\log(L_r/L)$ and $\log(\omega\tau_c)$ are also given.

Fig. 4.— The same as Fig. 3, but for first, third and fifth overtones, The effective temperature of corresponding static model is $T_e = 2550K$.

Fig. 5.— The variations of the pulsation periods P and the pulsation constants Q for the fundamental mode and the first overtone, against the effective temperature. The coupling between convection and oscillations is included.

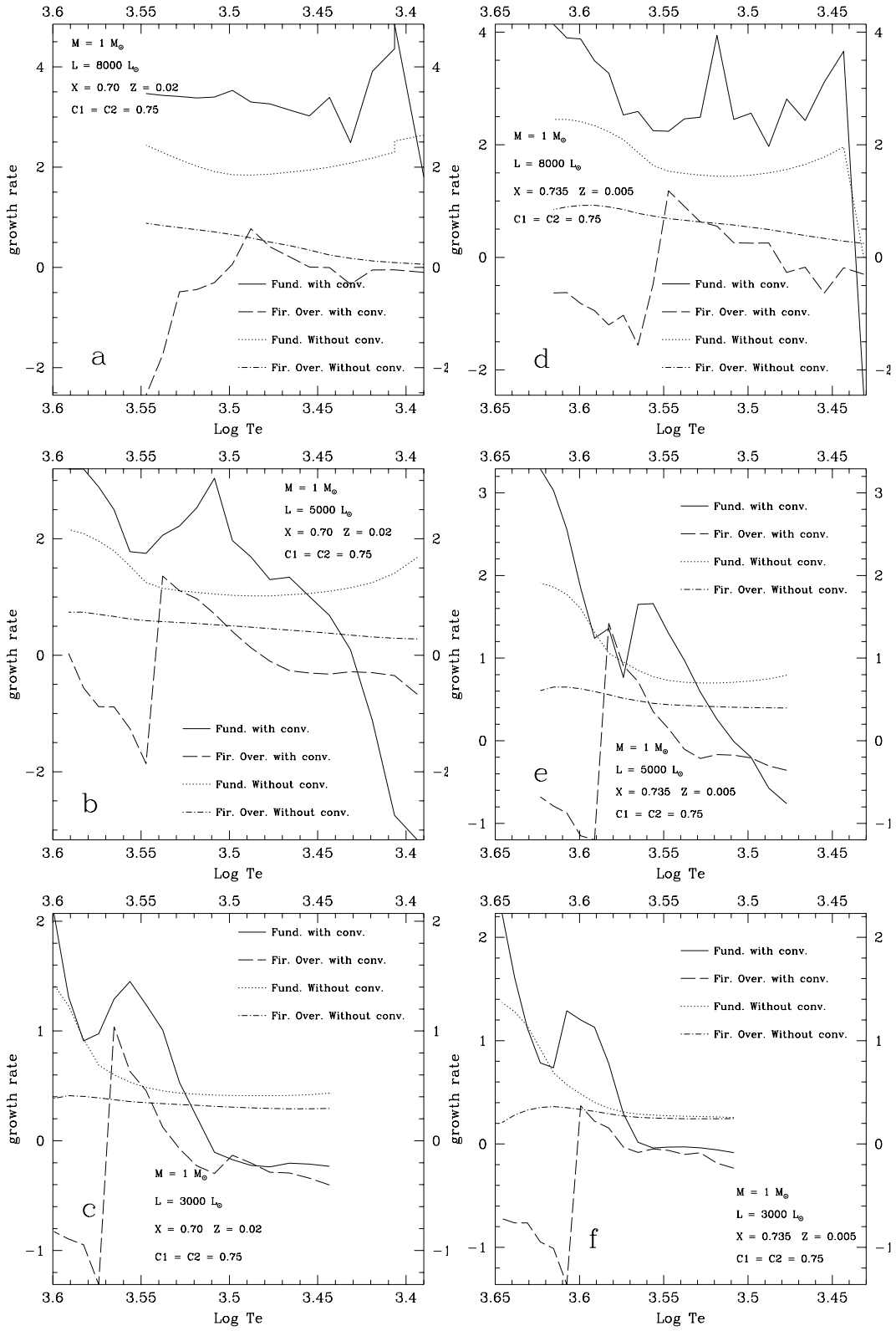


Fig. 1.—

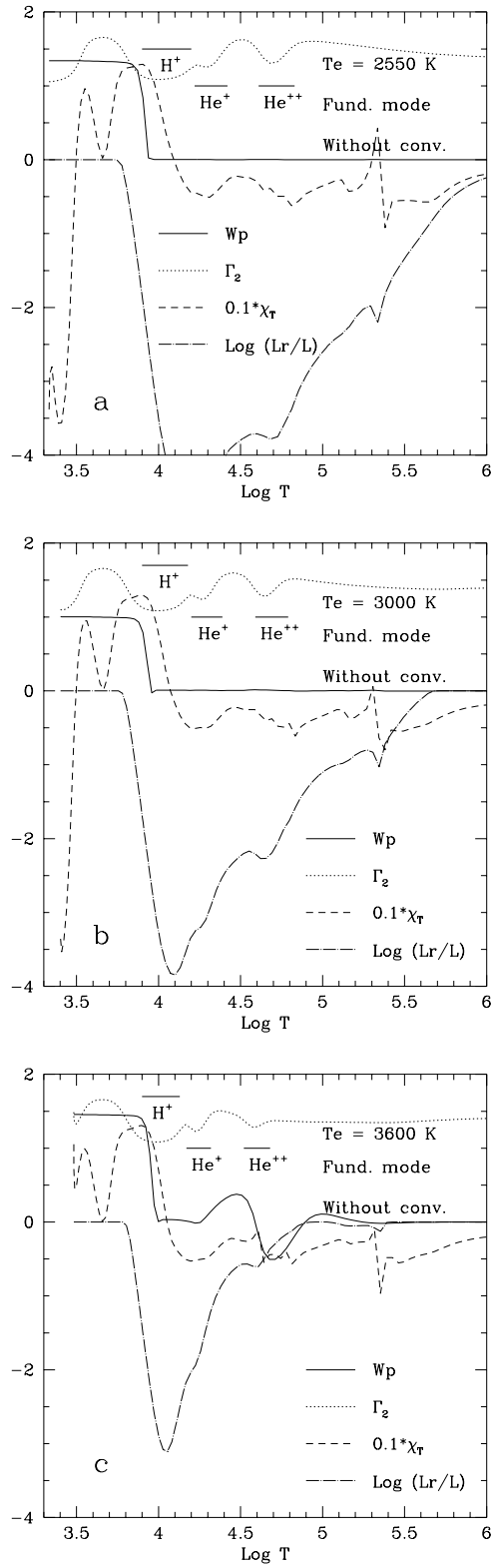


Fig. 2.—

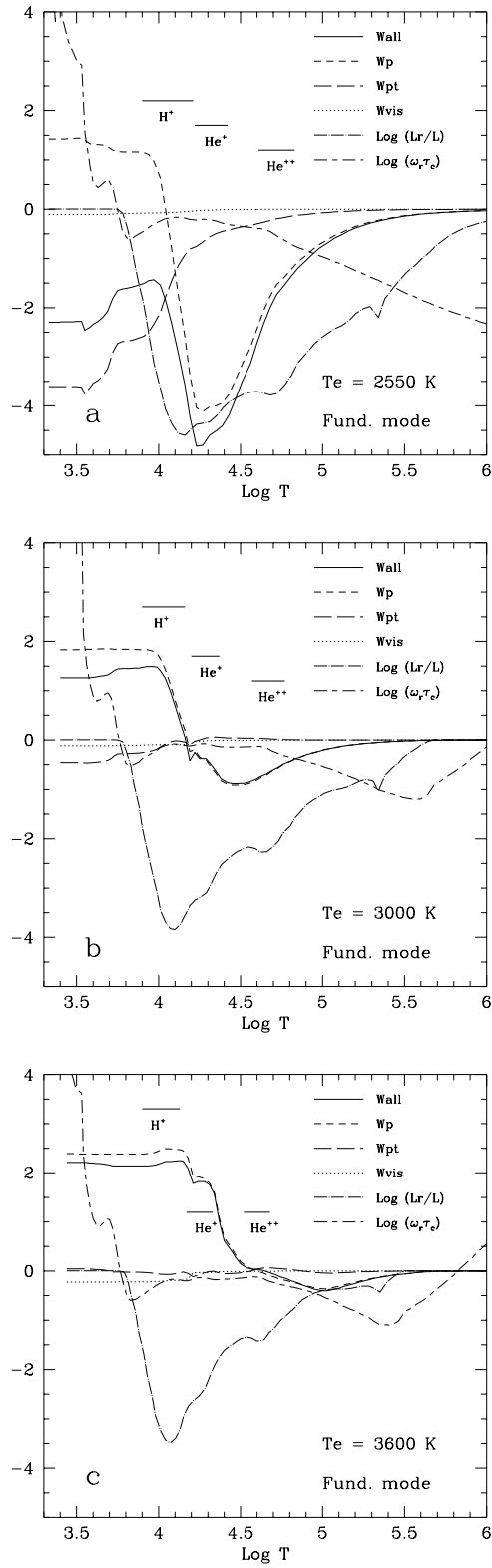


Fig. 3.—

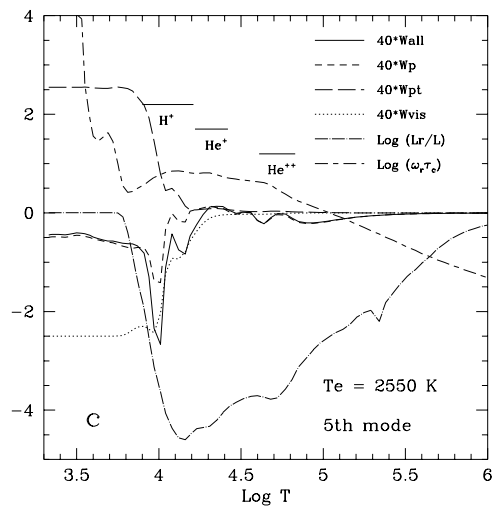
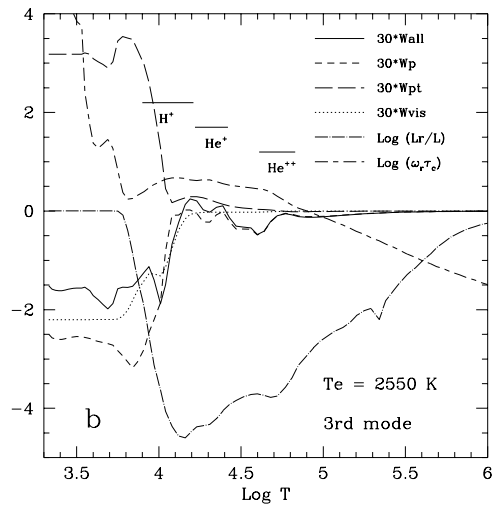
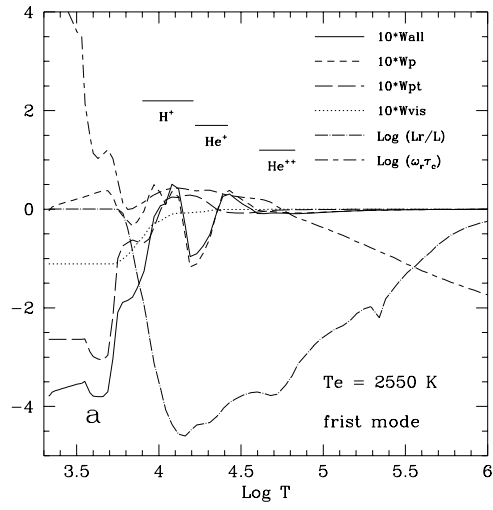


Fig. 4.—

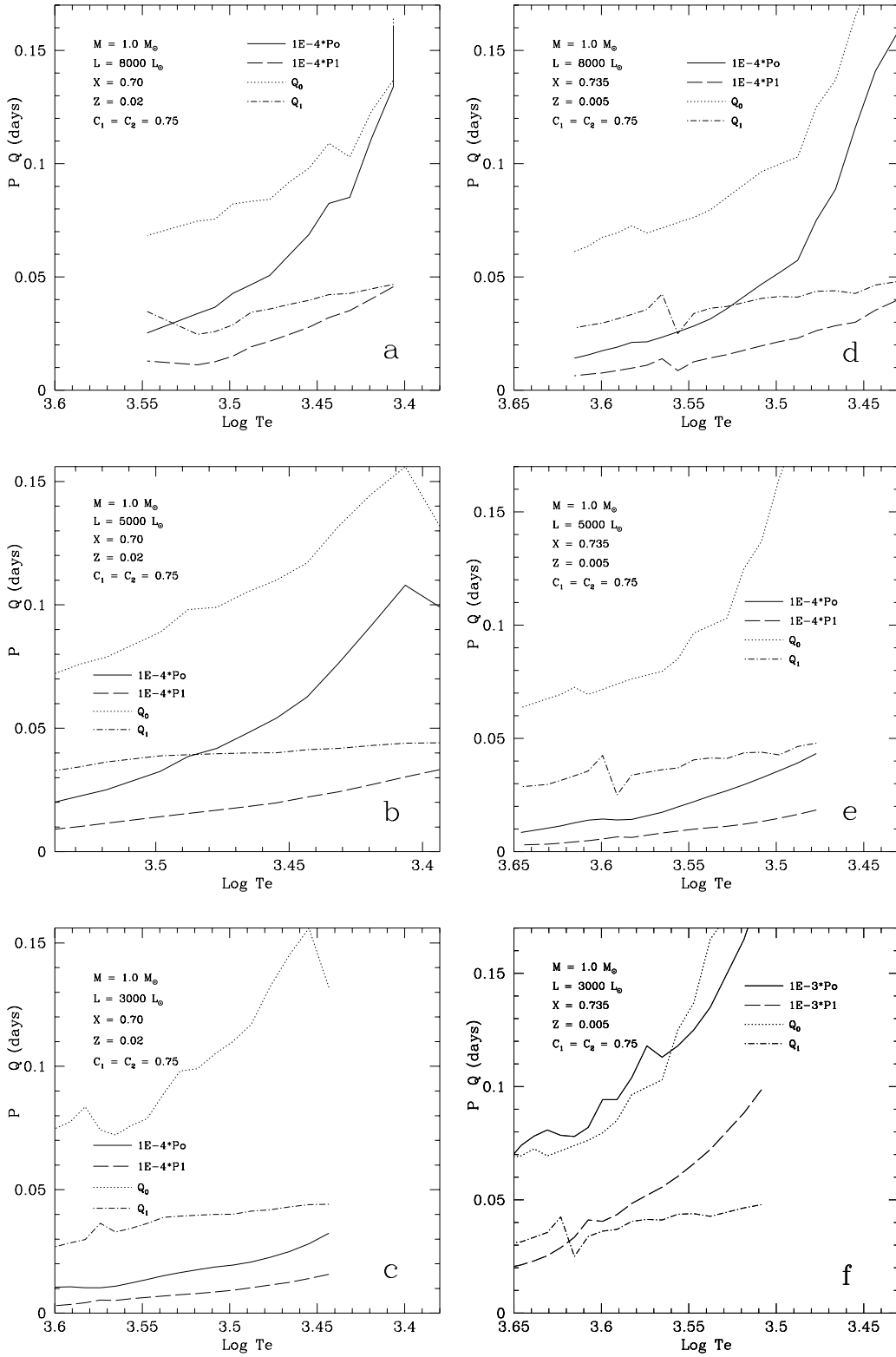


Fig. 5.—

Table 1. Pulsational instability strip (PIS)

no	M/M_{\odot}	L/L_{\odot}	X	Z	pulsational instability strip	
					F-mode	1st overtone
1	1.0	8000	0.70	0.02	~2300K -	2820 - 3190K
2	1.0	5000	0.70	0.02	2660K -	3040 - 3490K
3	1.0	3000	0.70	0.02	3260K -	3420 - 3720K
4	1.0	8000	0.735	0.005	2740K -	3040 - 3560K
5	1.0	5000	0.735	0.005	3260K -	3490 - 3860K
6	1.0	3000	0.735	0.005	3790K -	3790 - 4010K

Table 2. Amplitude growth rates for the first 5 modes
 $M = 1.0M_{\odot}$, $L = 5000L_{\odot}$, $X=0.70$, $Z=0.02$

with dynamic coupling of convection							without convection		
no	Te	η_0	η_1	η_2	η_3	η_4	η_0	η_1	η_2
1	2475.0	-----	-0.670D+00	-0.335D+00	-0.317D-01	-0.271D+00	0.168D+01	0.281D+00	0.115D
2	2550.0	-0.275D+01	-0.348D+00	-0.181D+00	-0.437D-01	-0.185D+00	0.141D+01	0.292D+00	0.950D
3	2625.0	-0.112D+01	-----	-0.154D+00	-0.783D-01	-0.165D+00	0.125D+01	0.314D+00	0.679D
4	2700.0	0.917D-01	-0.281D+00	-0.853D-01	-0.120D+00	-0.117D+00	0.116D+01	0.348D+00	0.327D
5	2775.0	-----	-0.324D+00	-0.330D-01	-0.143D+00	-0.758D-01	0.110D+01	0.378D+00	0.802D
6	2850.0	0.101D+01	-0.304D+00	-0.270D-01	-0.186D+00	-0.399D-01	0.106D+01	0.406D+00	-0.849D
7	2925.0	0.134D+01	-0.262D+00	-0.332D-01	-0.206D+00	-0.232D-01	0.104D+01	0.433D+00	-0.143D
8	3000.0	0.130D+01	-0.999D-01	-0.534D-01	-0.188D+00	-0.270D-01	0.102D+01	0.459D+00	-0.673D
9	3075.0	0.169D+01	0.131D+00	-0.781D-01	-0.159D+00	-0.397D-01	0.102D+01	0.482D+00	0.172D
10	3150.0	0.197D+01	0.406D+00	-0.117D+00	-0.135D+00	-0.516D-01	0.103D+01	0.504D+00	0.466D
11	3225.0	-----	0.712D+00	-0.121D+00	-0.115D+00	-0.957D-02	0.105D+01	0.525D+00	0.865D
12	3300.0	0.253D+01	-----	-0.864D-01	-0.239D+00	0.368D-02	0.108D+01	0.545D+00	0.115D
13	3375.0	0.222D+01	0.111D+01	-----	-0.211D+00	-0.792D-02	0.111D+01	0.561D+00	0.143D
14	3450.0	0.206D+01	0.136D+01	-0.202D+00	-0.140D+00	-0.462D-01	0.115D+01	0.577D+00	0.147D
15	3525.0	0.175D+01	-----	-0.177D+00	-0.448D-01	-0.916D-01	0.125D+01	0.593D+00	0.144D
16	3600.0	0.178D+01	-----	-----	0.555D-01	-0.177D+00	0.153D+01	0.624D+00	0.107D
17	3675.0	0.250D+01	-0.887D+00	0.185D+00	-0.760D-01	-0.361D+00	0.179D+01	0.668D+00	0.511D
18	3750.0	0.289D+01	-----	0.119D+00	-0.434D-01	-0.165D+00	0.196D+01	0.703D+00	-0.887D
19	3825.0	0.320D+01	-----	-0.142D+00	0.345D-01	-0.255D+00	0.209D+01	0.740D+00	-0.102D
20	3900.0	0.320D+01	-----	-0.632D+00	0.576D-01	-0.437D+00	0.216D+01	0.739D+00	-0.195D

Table 3. Pulsation period P and Q values for the first 5 modes
 $M = 1.0M_{\odot}$, $L = 5000L_{\odot}$, $X=0.70$, $Z=0.02$

no	Te	Period (days)					Pulsation co	
		P ₀	P ₁	P ₂	P ₃	P ₄	Q ₀	Q ₁
1	2475.0	-----	0.332D+03	0.263D+03	0.192D+03	0.160D+03	-----	0.441D-01
2	2550.0	0.108D+04	0.303D+03	0.232D+03	0.171D+03	0.140D+03	0.156D+00	0.440D-01
3	2625.0	0.918D+03	-----	0.206D+03	0.152D+03	0.123D+03	0.145D+00	-----
4	2700.0	0.765D+03	0.243D+03	0.181D+03	0.135D+03	0.107D+03	0.132D+00	0.419D-01
5	2775.0	-----	0.221D+03	0.161D+03	0.121D+03	0.938D+02	-----	0.413D-01
6	2850.0	0.541D+03	0.198D+03	0.143D+03	0.108D+03	0.829D+02	0.110D+00	0.401D-01
7	2925.0	0.478D+03	0.182D+03	0.128D+03	0.959D+02	0.736D+02	0.105D+00	0.400D-01
8	3000.0	0.419D+03	0.168D+03	0.114D+03	0.850D+02	0.654D+02	0.990D-01	0.397D-01
9	3075.0	0.386D+03	0.155D+03	0.101D+03	0.753D+02	0.582D+02	0.981D-01	0.393D-01
10	3150.0	0.325D+03	0.142D+03	0.909D+02	0.670D+02	0.523D+02	0.889D-01	0.388D-01
11	3225.0	-----	0.140D+03	0.831D+02	0.593D+02	0.472D+02	-----	0.412D-01
12	3300.0	0.251D+03	-----	0.737D+02	0.547D+02	0.430D+02	0.788D-01	-----
13	3375.0	0.226D+03	0.102D+03	-----	0.508D+02	0.387D+02	0.760D-01	0.344D-01
14	3450.0	0.201D+03	0.912D+02	0.596D+02	0.475D+02	0.354D+02	0.722D-01	0.328D-01
15	3525.0	0.183D+03	-----	0.552D+02	0.441D+02	0.327D+02	0.703D-01	-----
16	3600.0	0.182D+03	-----	-----	0.420D+02	0.303D+02	0.742D-01	-----
17	3675.0	0.192D+03	0.686D+02	0.489D+02	0.378D+02	0.271D+02	0.836D-01	0.298D-01
18	3750.0	0.168D+03	-----	0.464D+02	0.355D+02	0.258D+02	0.776D-01	-----
19	3825.0	0.153D+03	-----	0.444D+02	0.334D+02	0.247D+02	0.749D-01	-----
20	3900.0	0.137D+03	-----	0.423D+02	0.308D+02	0.240D+02	0.711D-01	-----